

## Structural insight to mutated Y116S transthyretin by molecular dynamics simulation

Avik Banerjee<sup>1</sup>, Hridoy R Bairagya<sup>1</sup>, Bishnu P Mukhopadhyay<sup>1\*</sup>, Tapas K Nandi<sup>1</sup> and Asim K Bera<sup>2</sup>

<sup>1</sup>Department of Chemistry, National Institute of Technology-Durgapur, West Bengal, Durgapur 713209, India

<sup>2</sup>Center for Advanced Research in Biotechnology, Rockville, Maryland 20850, USA

Received 11 November 2009; revised 09 June 2010

Familial amyloidotic polyneuropathy (FAP) is strictly associated with point mutations of transthyretin (TTR) protein. The Tyr116→Ser (Y116S) mutant TTR is an important amyloidogenic variant responsible for FAP. Structural dynamics of monomeric TTR and its mutant (Y116S) may give some clue relating to amyloid formation. In this study, molecular dynamic simulation at 310 K has been performed on wild-type and mutant (Y116S) TTR monomer, which can provide the molecular insight of structural transition in the inner and outer strand of the protein. Results show that mutation in the H-strand (Tyr116→Ser) leads to disruption of secondary structure and H-bonding pattern of some important parts of the inner DAGH-sheet of the protein. Especially, the residues T106, A108, L110 of G-strand, S117 and T119 of H-strand are affected, which are involved in the binding of thyroxin hormone. This unfolding of mutant structure during dynamics may cause instability in the protein and thus induce amyloidogenesis.

**Keywords:** Human transthyretin, Molecular dynamics simulation, Amyloid, Fibrils

Human transthyretin (TTR) is a plasma protein associated with the transportation of thyroid hormone and vitamin A<sup>1-4</sup>. The protein (TTR) has been found to form amyloid fibrils<sup>5</sup> and accumulates in tissues or extra-cellular matrix to cause amyloid diseases<sup>6</sup>. Two types of amyloid diseases, senile systemic amyloidosis (SSA) and familial amyloid polyneuropathy (FAP) are putatively caused by the amyloid deposition of wild-type transthyretin (WT-TTR) and its mutant variants in heart, peripheral nerves and other organs, causing autonomic and peripheral neuropathy, carpal tunnel syndrome, vitreous deposition, leptomeningeal amyloid and cardiomyopathy<sup>7,8</sup>.

Biologically active form of TTR is a homo-tetramer with 127 residues per monomer. The structures of the wild-type and various amyloidogenic single-site mutants have been determined by X-ray crystallography<sup>9-11</sup>. In the native state of TTR monomer, eight  $\beta$ -strands (A to H) are organized into

two sheets, where inner sheet is composed of D, A, G, H strands and outer sheet is composed of C, B, E, F strands, which give rise to a  $\beta$ -sandwich structure<sup>9,12</sup> (Fig. 1).

Several biochemical studies have revealed a multi-step assembly pathway of TTR amyloid fibril formation, where TTR tetramer first dissociates into native monomers and involves in the rate-limiting step of fibril formation<sup>13-16</sup>. Subsequently, the monomeric species partially unfold to form the aggregation intermediates and follow the self-

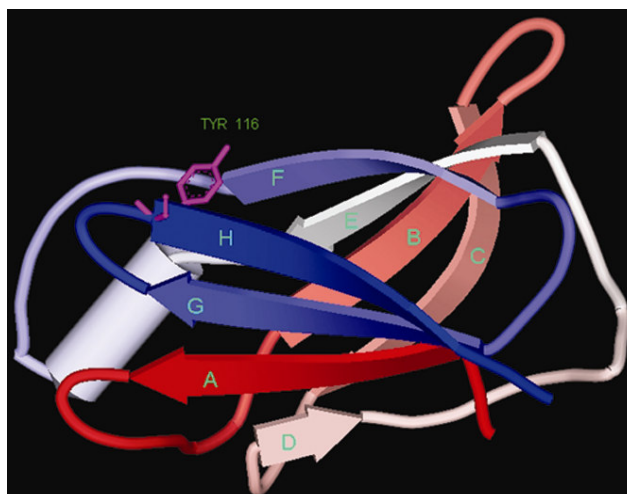


Fig. 1—Three-dimensional structure of wild type transthyretin monomer (PDB code: 1F41, A-Chain)

\*Corresponding author.

Tel: 0091-0343-2547074;

Fax: 0091-0343-2547375/2546753

E-mail: bpmk2@yahoo.com

**Abbreviations:** FAP, familial amyloidotic polyneuropathy; fs, femtosecond; MD, molecular dynamics; ns, nanosecond; ps, picosecond; RMSD, root mean square deviation; SASA, solvent accessible surface area; TTR, transthyretin; VMD, visual molecular dynamics; WT, wild type.

assembly process of polymerization<sup>17</sup>. Dissociation of tetramer into monomers is necessary, but not sufficient to initiate fibril formation because native monomers are non-amyloidogenic, unless their secondary and tertiary structures change substantially<sup>18</sup>. These tertiary structural changes can be facilitated either by partial denaturation<sup>16-20</sup> or by single-point mutation<sup>21,22</sup>.

Extensive biochemical studies have clearly revealed that Y116S mutant TTR is potentially responsible for FAP<sup>23,24</sup>, which is expressed by the predominant clinical features like peripheral neuropathy and carpal tunnel syndrome. The residue Y116 is located in the H-strand of the wild-type and plays an important role in dimer and tetramer formation<sup>25</sup>. Single-point mutation at this point (Y116S) perturbs the secondary, tertiary, and quaternary structures by disrupting the monomer-monomer and dimer-dimer interactions, which in turn accelerates amyloidogenesis by destabilizing the partially unfolded amyloidogenic intermediate state. But, till now the X-ray structure of Y116S-mutant TTR is not available in the protein data bank and no such computational or in-silico analysis has been carried out.

In the present study, the stability and flexibility of the wild-type (WT), and Y116S TTR monomer have been investigated using molecular dynamics (MD) simulations, which may provide an insight into the conformational changes during the early stage of TTR amyloid formation.

## Materials and Methods

### PDB structure

The structure of transthyretin has been taken from the protein data bank (PDB code: 1F41)<sup>26</sup>. The human TTR structure 1F41 has been found to crystallize as dimer (chains A and B). The chain A was separated using Swiss PDB Viewer program<sup>27</sup>.

### Mutation

Until now, no X-ray structure of Y116S mutant of transthyretin is available in the protein data bank. So, for our computational study, residue Tyr116 of wild-type TTR was mutated in-silico<sup>28</sup> to serine using the Swiss PDB Viewer program and the lowest energy rotamer for the mutated residue was chosen.

### Solvation

The wild-type (X-ray) and mutant (in-silico) structures were solvated in rectangular boxes (60 Å

× 50 Å × 50 Å) with 5010 water molecules by TIP3P model<sup>29</sup> using solvate plug-in program implemented in VMD.

### MD simulation

Solvated structures were initially energy-minimized (2000 cycles for all atoms to eliminate initial bad contacts which would destabilize the system) using the CHARMM force field<sup>30</sup>. After energy minimization, all the aquated structures were simulated using auto-interactive molecular dynamics (IMD) connected between the visualization program Visual Molecular Dynamics v. 1.8.6<sup>31</sup> and the MD program Nanoscale Molecular Dynamics v. 2.6<sup>32,33</sup>.

Each MD simulation was carried out for 10 ns at constant temperature 310 K and constant pressure 1 bar. The integrated time-step was limited to 2 fs<sup>36</sup> (which is much smaller than the fastest vibrational period of linear bonds involved to small hydrogen atoms) by means of Langevin dynamics using the CHARMM force field. The system was constructed using the periodic boundary conditions. The MD simulations were performed in the canonical N, P, and T ensemble. Trajectories were generated after 20 ps equilibration period at 310 K.

### Free energy calculation of protein

The stability free energy ( $\Delta G_s$ ) of the solvated X-ray, mutant and their MD-simulated structures were calculated using the program FOLDX<sup>34</sup>. The temperature, ionic strength, pH and VDW (parameters of FOLDX) were assigned as 310 K, 0.05 M, 7.0 and 2, respectively.

### Structural analysis

Trajectories during simulation were analyzed using VADAR (volume area dihedral angle reporter) program<sup>35</sup>. Parameters were the C $\alpha$  root mean square (RMS) deviations from the template structures, solvent accessible surface area (SASA), folding free energy ( $\Delta G_f$ ) and percentage of secondary structure etc.

## Results and Discussion

During 10 ns MD simulation, the secondary structure and H-bonding pattern of DAGH strands of the mutant Y116S monomer are largely disrupted compared to the wild-type TTR (WT-TTR). The profiles of RMSD during simulation appear to reach plateau after around 3.5 ns (Fig. 2), indicating the statistical convergence of the WT and mutant structures. Stability free energy of the systems also

reach plateau almost at the same time. Hence in the following analysis, we have collected snapshots during the last 6.5 ns. The mutant Y116S monomer shows larger  $C\alpha$  RMS deviation and higher stability free energy ( $\Delta G_s$ ) compared to WT-TTR over the last 6.5 ns. After convergence, RMSD of the WT-TTR varies between 1.2 to 1.6 Å, while that of the mutant Y116S varies between 1.7 to 2.1 Å.

The maximum, minimum and mean percentage of  $\alpha$ -helix,  $\beta$ -strand, and turn and random coil contents of the residues 10-125 for both the WT and mutant structures are included in Table 1. The residues 1-9 and 126,127 have not been considered because they are not resolved in the X-ray structure (PDB code: 1F41). Here the percentage of  $\beta$ -strand gradually decreases, destroying the compactness of the structures along the simulation trajectories. We observe that  $\beta$ -strand is 59% in the X-ray structure of TTR (1F41), while in MD averaged structure  $\beta$ -strand is 56.5% in WT-TTR monomer and 53.2% in mutant Y116S.

During the last 6.5 ns simulation of Y116S-TTR monomer, H-bonding pattern of the backbone amide

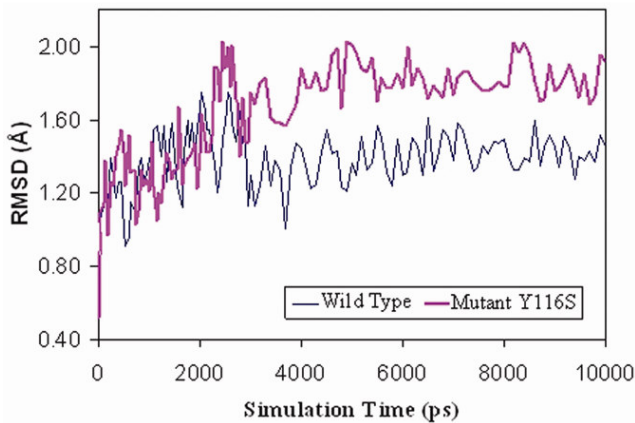


Fig. 2—The  $C\alpha$  root mean square deviation (RMSD) of the MD-simulated structures from the template structure

groups in the  $\beta$ -sandwich region has largely been changed. Hydrogen bond occupancy (last 6.5 ns of simulation) is included in Table 2. For both the proteins, most of the H-bonds connecting the C-, B-, E-, and F-strands are persistent, with more than 95% occupancy. Only one unstable H-bond is found between the E and F-strands in the Y116S-TTR monomer i.e., I73 (O) --- A91 (HN) with occupancy 84.7%. But in DAGH sheet, some of the H-bond connecting the A-, G-, and H- strands are broken or showing low persistency in the Y116S-TTR monomer and it is in consistent with the secondary structure fluctuation. The H-bonds, P11(O)---Y105 (HN), T106 (O)---V121 (HN) and L111(O)---A19 (HN), connecting the A- and G-strands in Y116S-TTR monomer seem relatively infrequent with occupancy 48.9%, 83.3% and 76.7% respectively (Table 2). The results also reveal that the H-bonds between the G- and H-strands involving A108(O) --- T119 (HN), L110(O) --- S117 (HN), T119(O) --- A108 (HN), and S117(O) --- L110 (HN) of the Y116S-TTR monomer have been completely broken. It is also observed that the spanning of  $\beta$ -strands (A-H) are rather conserved with some small fluctuations in WT-TTR monomer, whereas in the mutant Y116S structure, the strands A and H have become much shorter in length during simulation, though the strands from B to G have not changed much. The A-strand spanning from residue 11-19 in WT-TTR structure has become 13-18 in the mutant and it is prominent after 4500 ps. In case of H-strand, residues 115-123 in WT-TTR become confined between the residues 121-123 in the mutant after 1500 ps (Fig. 3). This shortening of strands may account for the reduction of percentage of  $\beta$  content and increase in coil content in mutant structure.

To reveal the influence of single-point mutations on the hydrophobicity/hydrophilicity of protein, we have calculated the total solvent accessible surface

Table 1—Secondary structure of WT and Y116S mutant TTR monomers during simulation

Simulation time (ns)		WT				Y116S			
		$\beta$ -strand (%)	Helix (%)	Turn (%)	Coil (%)	$\beta$ -strand (%)	Helix (%)	Turn (%)	Coil (%)
3.5–0	Avg.	56.5	6.4	7.3	29.8	53.1	6.4	6.1	34.4
	Max.	63.0	10.0	13.0	36.0	63.0	10.0	13.1	43.0
	Min.	54.0	4.0	3.0	20.0	48.0	4.0	2.0	20.0
3.5–7	Avg.	57.0	6.3	7.6	29.1	54.0	6.5	6.2	33.3
	Max.	63.0	10.0	13.0	36.0	63.0	10.0	13.0	43.0
	Min.	54.4	4.0	3.0	20.0	50.0	4.0	0.2	20.0
7–10	Avg.	55.7	6.3	6.9	31.1	52.1	6.2	6.0	35.7
	Max.	61.0	10.0	13.0	36.0	55.0	10.0	13.0	42.0
	Min.	54.0	5.0	3.0	23.0	50.0	4.0	3.0	25.0

Table 2—Hydrogen bond occupancy for the backbone atoms in the  $\beta$ -sheet region during the last 6.5 ns simulation

Strand	Acceptor	Donor	WT (%)	Y116S (%)
C & B	VAL 30	GLY 47	99.8	99.9
	VAL 32	PHE 44	99.8	99.7
	ARG 34	GLU 42	98.8	99.9
	GLU 42	ARG 34	99.4	98.5
	ALA 45	VAL 32	98.4	98.3
	GLY 47	VAL 30	98.0	96.0
B & E	HIS 31	GLU 72	99.6	99.3
	PHE 33	LYS 70	100.0	100.0
	ILE68	LYS 35	100.0	100.0
	LYS 70	PHE 33	99.9	99.9
E & F	GLU 72	HIS 31	98.6	99.9
	GLY 67	ALA 97	100.0	99.6
	TYR 69	PHE 95	100.0	100.0
	VAL 71	VAL 93	99.8	94.9
	ILE 73	ALA 91	99.8	84.7
	ALA 91	ILE 73	97.8	97.8
	VAL 93	VAL 71	99.8	98.9
	PHE 95	TYR 69	100.0	100.0
D & A	VAL 14	LEU 55	96.6	99.7
	GLY 53	VAL 16	100.0	100.0
A & G	PRO 11	TYR 105	99.0	48.9
	MET 13	ILE 107	99.4	94.9
	LYS 15	ALA 109	99.9	97.9
	LEU 17	LEU 111	100.0	99.7
	TYR 105	MET 13	99.9	88.8
	ILE 107	LYS 15	99.5	99.7
	ALA 109	LEU 17	97.3	99.5
	LEU 111	ALA 19	95.8	75.7
	G & H	ARG 104	THR 123	100.0
THR 106		VAL 121	97.3	83.3
ALA 108		THR 119	97.5	0.0
LEU 110		SER 117	95.7	0.0
LEU 110		SER 117	96.1	0.0
THR 119		ALA 108	95.4	0.0
VAL 121		THR 106	99.4	98.8
THR 123		ARG 104	100.0	100.0

area (SASA) of the molecules. It is observed that average SASA of the mutant monomer structure gradually increases along the trajectory as compared to WT-TTR (Fig. 4), indicating that after mutation the overall structure becomes more unfolded during the simulation.

Breaking of certain important H-bonds between the  $\beta$ -strands in mutant structure results in decrease in the number of main chain H-bonds (Fig. 5), leading to the increase in average inter-strand distance among them. This effect is most prominent between the A-G and G-H strand interface, where the increase in average inter-strand distance varies between 0.5 to 1 Å. Significant shifts are also seen near the beginning of B- and F-strands at the B-E and E-F interface. Again,

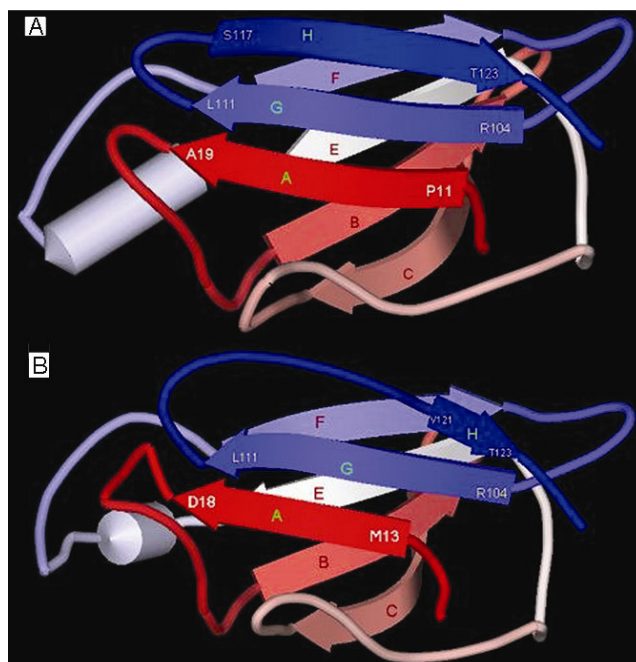


Fig. 3—(A): Three-dimensional structure of wild-type transthyretin monomer after 10 ns MD simulation; and (B): Three-dimensional structure of mutant (Y116S) transthyretin monomer after 10 ns MD simulation

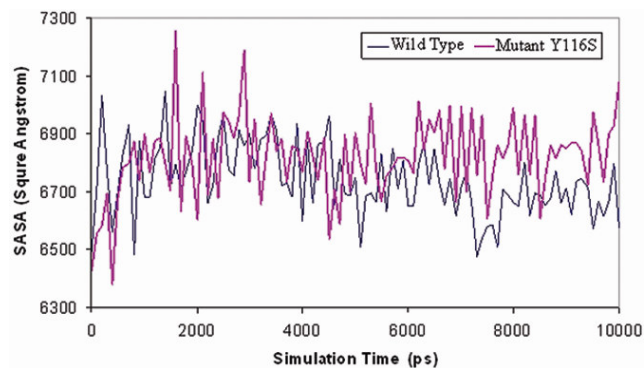


Fig. 4—Solvent accessible surface area (SASA) of wild-type and mutant (Y116S) transthyretin monomer during simulation

the B-C, F-G and G-H loops show large deviation for the mutant TTR with respect to the initial structure during simulation (Fig. 6). These shifts of strands ultimately result in unfolding of the structure that may also account for the increase in average SASA of the mutant structure.

Instability of the mutant protein molecule over the WT-TTR is also revealed in their stability free energy ( $\Delta G_s$ ) and folding free energy ( $\Delta G_f$ ) values along the trajectories (Fig. 7). Stability free energy may provide a quantitative estimation of important interaction e.g., electrostatic interaction, intra-molecular hydrogen bonding etc., which are contributing to the stability of

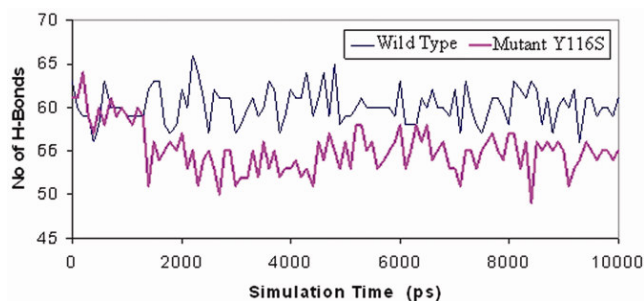


Fig. 5—Number of H-bonds between the backbone amide groups of wild-type and mutant (Y116S) transthyretin monomer during simulation

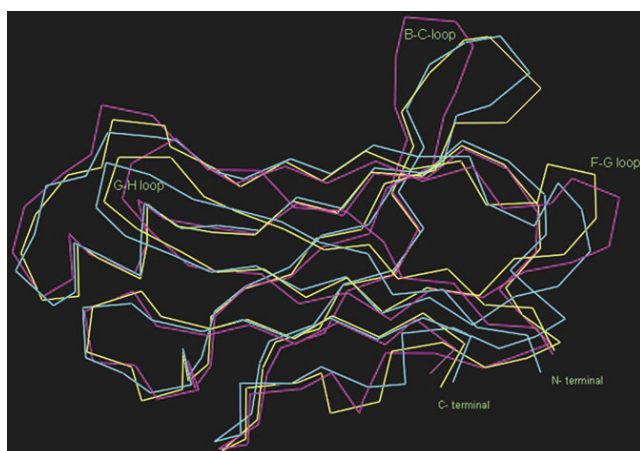


Fig. 6—Superposition of the  $\alpha$ -carbons of the initial X-ray (wild type) [blue], the MD-equilibrated (wild type) [yellow] and MD-equilibrated mutant (Y116S) [pink] structures

the respective proteins, whereas folding free energy<sup>35</sup> indicates the hydrophobic free energy contribution involved in the whole folding process of protein. Mean value of the  $\Delta G_s$  for the WT-TTR monomer is  $73.75 \pm 8.5$  kcal/mole, which is significantly lower than the mean value  $90.25 \pm 9.2$  kcal/mole of Y116S TTR. Again the mean value of  $\Delta G_f$  for the WT-TTR monomer appears to be  $-96.8 \pm 3.9$  kcal/mole, which is significantly lower than the mean value  $-90.7 \pm 3.4$  kcal/mole of Y116S-TTR. These results suggest that the packing between the CBEF and DAGH sheets is more compact in WT-TTR monomer compared to that of mutant Y116S.

Detailed biophysical studies (free energy, RMSD of backbone carbon atoms, SASA of all the structures during dynamics, main chain H-bonding and secondary structural analysis) have clearly explored that the solvated mutant structure is more unstable than its wild-type (PDB) structure. Thus, the present computational approach with detailed structural analysis (by mutating the residue Y116 to S116) may provide a better insight for the structural biochemistry of TTR protein in future.

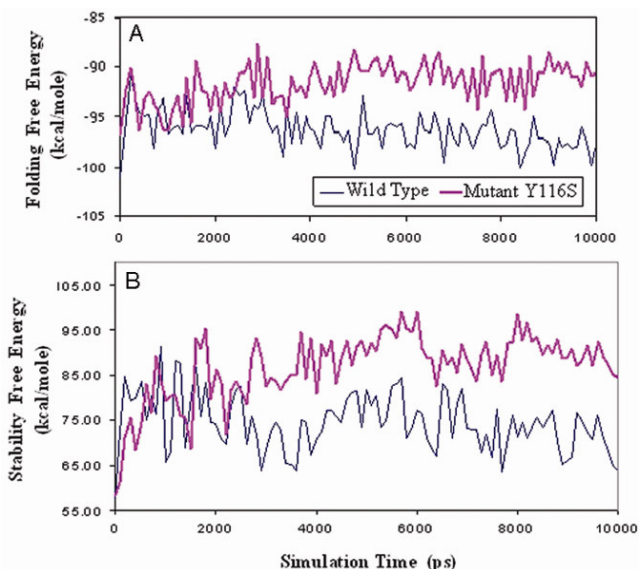


Fig. 7—(A): Folding free energy of wild-type and mutant TTR monomer during simulation; and (B): Stability free energy of wild-type and mutant TTR monomer during simulation

## Conclusion

The mutation of Tyr116 by Ser in TTR monomer results in substantial structural changes relative to WT-TTR during 10 ns simulation. The disruption of secondary structure and H-bonding pattern of DAGH strands in the Y116S monomer indicates the instability of mutant protein, which may further induce the amyloidogenesis. Also, the structural changes have been found to disturb the H-bonding dynamics of the residues T106, A108, L110 of the G-strand and S117 and T119 of the H-strand, which are specially involved in the binding of thyroxin molecule.

## Acknowledgements

Authors acknowledge to National Institute of Technology (Govt. of India), Durgapur for providing the TEQIP research facilities.

## References

- Robbins J & Rall J E (1957) *Recent Prog Horm Res* 13, 161-202
- Oppenheimer J H (1968) *N Engl Med* 278, 1153-1162
- Peterson P A (1971) *J Biol Chem* 246, 44-49
- Kanai M, Raz A & Goodman D S (1968) *J Clin Invest* 47, 2025-2044
- Sacchetti J C & Kelly J W (2002) *Nat Rev Drug Discov* 1, 267-275
- Koo E H, Lansbury P T & Kelly J W (1999) *Proc Natl Acad Sci (USA)* 96, 9989-9990
- Hou X, Aguilar M I & Small D H (2007) *FEBS J* 274, 1637-1650
- Goh K J, Kim J H, Kim B J & Tan C T (2008) *Neurol Asia* 13, 121-124

- 9 Blake C C, Geisow M J, Oatley S J, Rerat B & Rerat C (1978) *J Mol Biol* 121, 339-356
- 10 Hamilton J A, Steinrauf L K, Braden B C, Liepnieks J, Benson M D, Holmgren G, Sandgren O & Steen L (1993) *J Biol Chem* 268, 2416-2424
- 11 Sebastiao M P, Saraiva M J & Damas A M (1998) *J Biol Chem* 273, 24715- 24722
- 12 Yang M, Lei M, Bruschiweiler R & Huo S (2005) *Biophys J* 89, 433-443
- 13 Steward R E, Armen R S & Daggett V (2008) *Protein Engg Design Selection* 21, 187-195
- 14 Hammarstrom P, Schneider F & Kelly J W (2001) *Science* 293, 2459-2462
- 15 Schneider F, Hammarstrom P & Kelly J W (2001) *Protein Sci* 10, 1606-1613
- 16 Hammarstrom P, Jiang X, Hurshman A R, Powers E T & Kelly J W (2002) *Proc Natl Acad Sci (USA)* 99 (Suppl 4), 16427-16432
- 17 Hurshman A R, White J T, Powers E T & Kelly J W (2004) *Biochemistry* 43, 7365-7381
- 18 Jiang X, Smith C S, Petrassi H M, Hammarstrom P, White J T, Sacchettini J C & Kelly J W (2001) *Biochemistry* 40, 11442-11452
- 19 Colon W & Kelly J W (1992) *Biochemistry* 31, 8654-8660
- 20 Lashuel H A, Lai Z, & Kelly J W (1998) *Biochemistry* 37, 17851-17864
- 21 Hsu L C, Hsu N C, Guzova J A, Guzov V M, Chang S F & Chung B (1996) *J Biol Chem*, 271, 3306-3310
- 22 Singh D, Raman B, Ramakrishna T & Rao C M (2006) *Mol Vision* 12, 1372-1379
- 23 Hornberg A, Eneqvist T, Olofsson A, Lundgren E & Sauer-Eriksson A E (2000) *J Mol Biol* 302, 649-669
- 24 Skoulakis S & Goodfellow J M (2003) *Biophys J* 84, 2795-2804
- 25 Misrahi A M, Plante V, Lalu T, Serre L, Adams D, Lacroix D C & Said G (1998) *Hum Mutat* 12, 71-74
- 26 Plante-Bordeneuve V, Lalu T, Misrahi M, Reilly M M, Adams D, Lacroix C & Said G (1998) *Neurology* 51, 708-714
- 27 Guex N, Diemand A, Peitsch M C & Schwede T (2001) (Glaxo SmithKline R&D) Swiss PDB Viewer program
- 28 Dasgupta J, Sen U & Dattagupta J K (2003) *Protein Eng* 16, 489-496
- 29 Jorgensen W L (1982) *J Chem Phys* 77, 4156-4163
- 30 Brooks B R, Bruccoleri R E, Olafson B D, States D J, Swaminathan S, Karplus M (1983) *J Comput Chem* 4, 187-217
- 31 Humphrey W, Dalke A & Schulten K (1996) *J Mol Graph* 14, 33-38
- 32 Nelson M, Humphrey W, Gursoy A, Dalke A, Kale L, Skeel R D & Schulten K (1996) *Int J Supercomput Appl High Perform Comput* 10, 251-268
- 33 Phillips J C, Braun R, Wang W, Gumbart J, Tajkhorshid E, Villa E, Chipot C, Skeel R D, Kale L & Schulten K (2005) *J Comput Chem* 26, 1781-1802
- 34 Schymkowitz J, Borg J, Stricher F, Nys R, Rousseau F & Serrano L (2005) *Nucleic Acids Res* 33, 382-388
- 35 Willard L, Ranjan A, Zhang H, Monzavi H, Boyko R F, Sykes B D & Wishart D S (2003) *Nucleic Acids Res* 31, 3316-3319
- 36 Beck A C & Dagget V (2004) *Methods* 34, 112-120